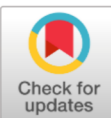


AIAA'86



AIAA-86-1308
Calculation of Convective Heating on
Proposed Aeroassist Flight
Experiment Vehicle

H.H. Hamilton and K.J. Weilmuenster,
NASA Langley Research Center,
Hampton, VA

**AIAA/ASME 4th Joint Thermophysics and
Heat Transfer Conference**

June 2-4, 1986/Boston, Massachusetts

CALCULATION OF CONVECTIVE HEATING ON PROPOSED
AEROASSIST FLIGHT EXPERIMENT VEHICLE

H. Harris Hamilton II* and K. James Weilmuenster†
NASA Langley Research Center
Hampton, Virginia 23665-5225

Introduction

To further exploit the opportunities in near and far space, a new family of vehicles, known as aeroassist vehicles, have been proposed. A review of several aeroassist vehicle concepts is given by Walberg in Ref. 1. These vehicles will typically operate in the upper reaches of the atmosphere at velocities higher than those usually encountered by other reentry vehicles and utilize their aerodynamic characteristics to assist in carrying out orbital maneuvers associated with their mission.

Of current interest is an aeroassist orbital transfer vehicle (AOTV) which will be used to transfer payload from low- to high-Earth orbit and back. In returning from high- to low-Earth orbit, this vehicle will use the upper atmosphere to assist its retro rockets in reducing the speed of the vehicle to Earth orbital velocity. This will decrease the amount of propellant required for this maneuver. Previous studies² have shown that a vehicle with an L/D in the range of at least 0.2 to 0.4 is required to carry out this mission effectively. Vehicles that exhibit this range of L/D fall into the class of very blunt bodies such as 60° to 70° sphere cones or other simple blunt shapes.

In order to better understand the flow field, pressure loads, aerodynamics, and heating on vehicles of this class under flight conditions, an aeroassist flight experiment (AFE) has been proposed by research organizations within the National Aeronautics and Space Administration. Although numerous body shapes have been considered, a configuration³ proposed by the Johnson Space Center appears to be a leading candidate for the flight experiment. This configuration is a blunted, elliptic cone raked off at the base. This forebody is fitted with a skirt-type afterbody having a generous corner radius to reduce the heating in the region of the forebody-afterbody juncture.

In the present paper, heating rates on this configuration, calculated by the method described in Refs. 4 and 5, will be presented in order to give the reader an understanding of the heating patterns to be expected on this type of vehicle. Comparisons will also be made with experimental data obtained in the Langley 31-Inch Mach 10 Tunnel. In this preliminary analysis, only wind-tunnel conditions will be considered.

*Research Leader, Aerothermodynamics Branch, Space Systems Division. Member AIAA.

†Aero-Space Technologist, Aerothermodynamics Branch, Space Systems Division. Member AIAA.

This paper is declared a work of the U.S. Government and is not subject to copyright protection in the United States.

Nomenclature

| | |
|---------------|---|
| C_p | pressure coefficient |
| C_M | pitching-moment coefficient |
| D | drag |
| D_r | diameter of rake plane |
| h | heat-transfer coefficient |
| L | lift and length of base in symmetry plane |
| M | Mach number |
| p | pressure |
| r | radius of skirt on AFE body |
| R_e | Reynolds number |
| s | surface distance measured from nose |
| T | temperature |
| z_c | juncture of ellipsoidal nose with elliptic cone on AFE body |
| α | angle of attack |
| γ | ratio of specific heats for ideal gas |
| δ | rake angle |
| ϵ_b | ellipticity of ellipsoid in yz plane |
| θ_{yz} | half-angle of elliptic cone in yz plane |
| τ | angular extent of circular arc in yz plane |

Subscripts:

∞ freestream

ref reference value

Geometry

The configuration considered in the present paper is one of a family of bodies proposed by the Johnson Space Center for the flight experiment. These bodies (illustrated in Fig. 1) are generated by an elliptic cone of half-angle θ_{yz} (in yz plane) which has been raked off at an

angle δ (measured relative to the cone axis). The nose of the body is made of an ellipsoid with ellipticity ϵ_b in the yz plane which is tangent to the cone at station z_c . This forebody is joined to a skirt-type afterbody which is generated by fitting an arc of radius r , which is tangent to the cone in each meridional plane. The arc sweeps through an angle of τ in the yz plane (Fig. 1). This reduces the flow expansion near the base of the cone and also reduces the heating in this region.

A particular body within this class of raked elliptic cones is completely defined by the five parameters θ_{yz} , ϵ_b , δ , r , and τ . For the present paper, the geometry considered has the following values for these parameters.

$$\begin{aligned}\theta_{yz} &= 60^\circ \\ \epsilon_b &= 2 \\ \delta &= 73 \\ r &= 0.10r \\ \tau &= 60^\circ\end{aligned}$$

In order to compute the inviscid flowfield over this configuration, the geometry has been altered by replacing the downstream portion of the skirt with a cylindrical afterbody as shown in Fig. 2. This was done to provide an afterbody extension for the upper part of the AFE geometry that would be convenient for computations. This alters the geometry of the skirt slightly, but has no effect on the upstream flow because the Mach number is already supersonic ahead of the cylindrical afterbody juncture. The computational geometry is shown in Fig. 2(b) and the actual geometry is shown in Fig. 2(a). Similar techniques have been used to compute the flowfield over other types of configurations with good success.

An analytic method of describing the raked elliptic cone bodies illustrated in Fig. 1 has been developed by Cheatwood and DeJarnette.⁶ This method provides a set of FORTRAN subroutines which can be included with any computer program. These subroutines will provide surface coordinates and derivatives for any of the class of raked, elliptic cone bodies illustrated in Fig. 1. They have been used in the present study to describe the AFE geometry.

Computational Techniques

The flowfield over the AFE configuration is computed using an inviscid method to first compute the outer flowfield and then using these results to supply edge properties to an approximate three-dimensional boundary-layer method to calculate the surface heating. Both the inviscid and boundary-layer methods are briefly described in the sections that follow.

Inviscid Flowfield Computations

The HALIS (High Alpha Inviscid Solution) inviscid flowfield code was initially developed to handle the high angle-of-attack flowfields about the shuttle vehicle, which were characterized by large embedded subsonic flow regions on the windward surface. Since, depending on each particular design, all or a

large portion of the aeroassist vehicle's surface, as well as its outer flowfield will be subsonic, the same methodology used for the shuttle can be used for the aeroassist vehicles.

The HALIS code is described in detail in Ref. 7. Briefly, the code is a time-asymptotic solution of the Euler equations which utilize an unsplit MacCormack differencing scheme. The solution space is the volume between the body surface and the bow-shock wave, which is treated as a time-dependent boundary. This leads to a coordinate system defined by the position of the bow shock and the body, as well as the spatial derivatives along these surfaces. The HALIS code uses a spherical coordinate system to describe the noscap region of the vehicle and is matched to a cylindrical coordinate system which describes the rest of the vehicle. For the present computations, the body is best described in the spherical system alone. Thus, a spherical-system version of HALIS has been created for this and similar studies. In addition, two new coordinate transformations have been added to the code. The first compresses the grid at the wall for greater radial resolution, and the second is used to distribute points in the θ direction for greater resolution of the flow at the body-skirt juncture.

The code is written in vector FORTRAN for the CDC VPS-32 computer and uses 64-bit words. Run times vary with configuration and angle of attack, but average approximately 25 minutes of CPU time for the present cases where the flowfields contain approximately 36,000 grid points.

Boundary-layer Solution

The surface heating rates are calculated using the axisymmetric analogue for three-dimensional boundary layers developed by Cookc.⁸ The details of the present method are described in Ref. 4. Briefly, the general, three-dimensional, boundary-layer equations are written along a streamline and are reduced to the axisymmetric form when the crossflow in the boundary layer is neglected--if the distance along a streamline is interpreted as the distance along an equivalent body and the metric that describes the spreading of the streamlines is interpreted as the radius of the equivalent axisymmetric body. This allows any axisymmetric boundary-layer solution to be used to calculate the approximate, three-dimensional, heating rates along streamlines, which greatly simplifies the problem. By considering multiple streamline paths, the heating over a complete vehicle can be computed at a fraction of the cost that would be required if the full, three-dimensional, boundary-layer equations were used.

In the present paper, the inviscid solution from HALIS is used to compute the streamline information and boundary-layer edge properties. No iteration is considered between the boundary layer and inviscid solutions, thus the Reynolds numbers must be reasonably large so that the boundary-layer solution does not strongly effect the inviscid solution. A rapid, approximate, integral method⁹ is used to calculate the heating along individual streamlines. Additional terms¹⁰

have been added to account for the large velocity gradients that occur near the beginning of the skirt which can significantly increase the heating in this region.

For all of the cases considered in the present paper, 91 streamlines were used to describe the heating over the body. Using this approach, each case required approximately 3 minutes of CPU time on a CDC CYBER 730 computer.

Results and Discussion

In this section, the discussion will first focus on the accuracy of the HALIS inviscid flowfield calculations for the AFE vehicle. Next, the inviscid streamlines will be presented and compared with oil-flow data. Finally, heat-transfer coefficients calculated using the axisymmetric analogue will be presented and compared with available wind-tunnel data for validation.

Flowfield

As we discussed previously, HALIS is used to compute the inviscid flowfield over the AFE configuration, and from this solution, edge properties are obtained for boundary-layer and heating calculations. In previous work,⁵ HALIS has been shown to provide accurate flowfield solutions for spherically blunted, 70° half-angle cones which have many similarities to the AFE flowfield. Experimental pressures are needed to help demonstrate the accuracy of the HALIS solutions for the AFE applications, but they are not presently available.

The HALIS code has been used to compute aerodynamic coefficients for the AFE and the results have been compared with experimental data.¹¹ A summary of those results for the pitching-moment coefficient is presented in Fig. 3. Results are shown for two test gases, air at $M_\infty = 10$ and CF₄ at $M_\infty = 6$. Although the pitching moments are quite different for the two gases, the HALIS calculations are in very good agreement in each case. The very good agreement between the HALIS calculations and the experimental data give confidence that the code can be used to make accurate flowfield calculations over the AFE vehicle.

Also shown in Fig. 3 are predicted pitching moments from Newtonian theory. It should be noted that these predictions do not agree with the experimental data for either of the test gases. Thus, Newtonian theory does not produce reliable results for the AFE vehicle.

Streamlines

The inviscid streamline pattern at $\alpha = 0^\circ$, 5° , and 10° are shown in Figs. 4, 5, and 6. These results were calculated at $M_\infty = 9.86$ and $\gamma = 1.4$. Also shown in the figure are photographs from oil-flow tests in the Langley 31-Inch Mach 10 Tunnel at the same flow conditions. As can be seen, the inviscid streamlines are in very good agreement with the experimental results. Both

sets of streamlines show the three-dimensional character of the flow, especially in the stagnation region. The stagnation point can be seen to move downward along the windward symmetry plane as the angle of attack is increased. There does appear to be slightly more curvature to the oil-flow traces on the more leeward portion of the body near the skirt, but this is not surprising since the oil-flow traces should be more affected by viscous forces in this region. Overall, the comparisons are very good.

Surface Heating

Heating calculations have been made over the AFE geometry for angles of attack from -10° to $+10^\circ$. All of the calculations were performed at the following flow conditions:

$$\begin{aligned} M_\infty &= 9.86 \\ p_\infty &= 1.256 \text{ Lbs/ft}^2 \\ T_\infty &= 94^\circ\text{R} \end{aligned}$$

which produced a freestream unit Reynolds number of approximately $0.5 \times 10^6/\text{ft}$. These calculated heat-transfer coefficients are compared with experimental data obtained in the 31-Inch Mach 10 Hypersonic Tunnel in Figs. 7-10 to help validate the present method and to show the types of heating distributions that will occur over this type of vehicle.

The results for $\alpha = 0^\circ$ are presented in Fig. 7. These data are presented as h/h_{ref} versus nondimensional surface distance measured from the nose of the body. The data on the left (Fig. 7(a)) are located in the pitch plane with positive values of s/L for the lower symmetry plane (Fig. 1) and negative values of s/L for the upper symmetry plane (Fig. 1). The data on the right (Fig. 7(b)) are located in a lateral plane passing through the nose.

The heating in the symmetry plane (Fig. 7(a)) decreases away from the stagnation point as would be expected. On the leeward symmetry plane, the decrease is very rapid for s/L values less than approximately -0.2 , and the heating is very low over the entire skirt. Along the windward symmetry plane, the heating decreases very rapidly at first, but levels out over the aft portion of the elliptic cone section (Fig. 1). As the skirt is approached, the heating increases and reaches a peak near $s/L = 0.77$. This increase in heating near the beginning of the skirt is the result of the rapid acceleration of the flow in that region. This is similar to the phenomenon that was noted in Ref. 5 for 70° spherically blunted cones. The data shown in the figure were obtained on moderate fidelity, stycast models using the phase-change paint technique, and its accuracy is probably + or -20 percent. Considering this accuracy, the present calculations are in very good agreement with the data.

The lateral heating decreases away from the symmetry plane and reaches a small plateau slightly ahead of the skirt. On the skirt, the heating falls continuously to a very low value near the base of the body. No peak is noted in the heating in the acceleration region ahead of

the skirt as was noted on the lower symmetry plane. The calculations are in good agreement with the experimental data.

The results for $\alpha = 5^\circ$ are presented in Fig. 8. These are very similar to those for $\alpha = 0^\circ$ shown in the previous figure except that the stagnation point has moved slightly downstream to a value of s/L of approximately 0.06. The calculations for this case are also in very good agreement with the experimental data.

The results for $\alpha = 10^\circ$ are presented in Fig. 9. The stagnation point for this case has moved even further downstream along the symmetry plane to a value of s/L of approximately 0.12. The agreement between the calculated and experimental data for this case is not as good as for the two lower angles of attack shown previously, but the agreement is still good except for the lateral distribution on the skirt (Fig. 9(b)). For this region, the calculations exhibit the correct qualitative behavior, but underpredict the experimental data by a large amount.

The results for $\alpha = -10^\circ$ are presented in Fig. 10. The stagnation point for this case has moved to the leeward symmetry plane to a value of s/L of approximately -0.06. The agreement between the calculations and the experimental data in the symmetry plane are the poorest of all of the cases considered in the present paper. However, the predictions still fall within the range of uncertainty for the experimental data. A slight rise is predicted in the heating in the lateral direction at the beginning of the skirt, but the rise is not as great as that exhibited by the experimental data. Overall, however, the agreement is still reasonably good.

Heating contours on the face of the AFE configuration for $\alpha = 0^\circ$, 5° , 10° , and -10° are presented in Figs. 11-14, respectively. These show many of the features of the heating on the AFE discussed previously and should give the reader a better understanding of the overall heating distributions on this vehicle. Of particular interest is the large region of relatively constant heating on the ellipsoidal nose surrounding the stagnation point and the large region of relatively constant heating on the lower portion of the elliptic cone segment ahead of the skirt. The heating on the skirt is relatively low.

Acknowledgments

The authors express their thanks to Bill Hinson and Charles Miller of the Experimental Aerodynamics Branch, Space Systems Division of the Langley Research Center for their assistance in making the experimental data presented in this paper available for publication.

Concluding Remarks

Heating calculations have been made on the AFE configuration at a Mach number of 9.86 and Reynolds number of approximately $0.5 \times 10^6/\text{ft}$ for angles of attack from -10° to 10° using an

approximate three-dimensional boundary-layer solution with edge conditions obtained from the HALIS flowfield code. These calculations are in good agreement with experimental data obtained in the Langley 31-Inch Mach 10 Tunnel and thus validate the present approach for calculating convective heating on the AFE vehicle. Heating contours are presented which show the overall heating patterns on the AFE configurations that should be useful in making initial determinations of the convective heating distributions that will occur on the actual vehicle. However, great care should be used in extrapolating heating data obtained in conventional, hypersonic wind tunnels to flight conditions because the character of the flowfield will be quite different due to real-gas effects.

References

¹Walberg, G. D., "A Survey of Aeroassisted Orbit Transfer," *Journal of Spacecraft and Rockets*, Vol. 22, No. 1, January-February 1985, pp. 3-18.

²Talay, T. A., White, N. W., and Naftel, J. C., "Impact of Atmospheric Uncertainties and Viscous Interaction Effects on the Performance of Aeroassisted Orbital Transfer Vehicles," *Thermal Design of Aeroassisted Orbital Transfer Vehicles; Progress in Astronautics and Aeronautics*, Vol. 96, edited by H. F. Nelson, AIAA, New York, 1985, pp. 198-229.

³Roberts, B. B., "Systems Analysis and Technology Development for the NASA Orbital Transfer Vehicle," AIAA Paper 85-0965, June 1985.

⁴Hamilton, H. Harris II, DeJarnette, Fred R., and Weilmuenster, K. James, "Application of Axisymmetric Analogue for Calculating Heating in Three-Dimensional Flows," AIAA Paper 85-245, January 1985.

⁵Weilmuenster, K. James and Hamilton, H. Harris II, "A Comparison of Computed and Experimental Pressure and Heating on 70° Sphere Cones at Angles of Attack to 20° ," AIAA Paper 86-0567, January 1986.

⁶Cheatwood, F. McNeil and DeJarnette, Fred R., Hamilton, H. Harris II, "Geometrical Description for a Proposed Aeroassist Flight Experiment Vehicle," NASA TM 87714, March 1986.

⁷Weilmuenster, K. James and Hamilton, H. Harris II, "Calculations of Inviscid Flow Over Shuttle-Like Vehicles at High Angles of Attack and Comparisons with Experimental Data," NASA TP 2103, May 1983.

⁸Cooke, J. C., "An Axially Symmetric Analogue for Three-Dimensional Boundary Layers," R. & M. No. 3200, British A.R.C., 1961.

⁹Zoby, E. V., Moss, J. N., and Sutton, K., "Approximate Convective Heating Equations for Hypersonic Flow," *Journal of Spacecraft and Rockets*, Vol. 18, January 1981, pp. 64-70.

¹⁰Kemp, Nelson, Rose, Peter H., and Detra, Ralph W., "Laminar Heat Transfer Around Blunt Bodies in Dissociated Air," *Journal of Aerospace Sciences*, Vol. 26, July 1959, pp. 421-430.

¹¹Weilmuenster, K. James and Hamilton, H. Harris II, "A Comparison of Computed and Measured Aerodynamic Characteristics of a Proposed Aeroassist Flight Experiment Configuration," AIAA Paper 86-1366, June 1986.

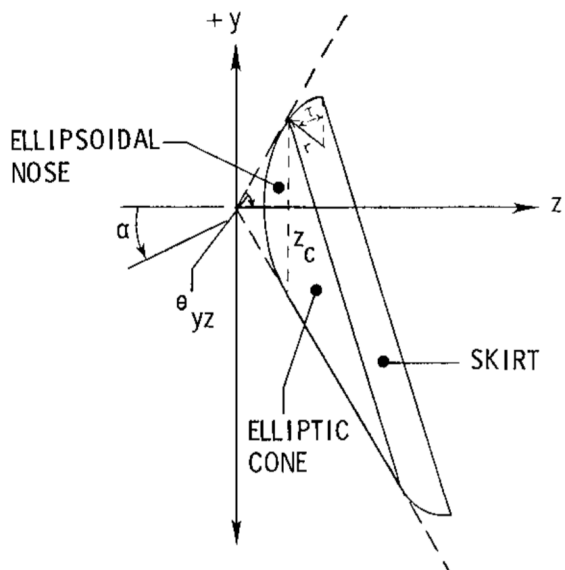


Fig. 1 Geometry of raked-elliptic cone.

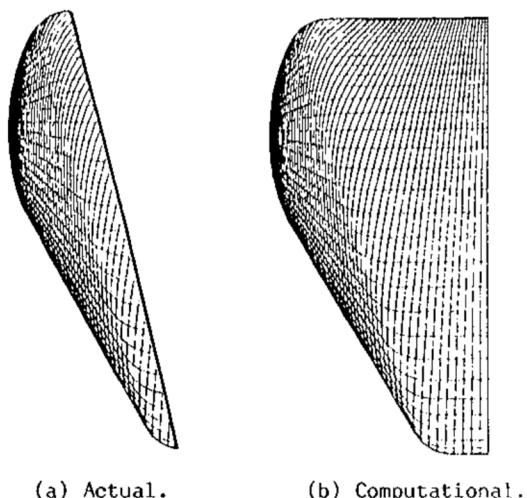


Fig. 2 AFE computational geometry.

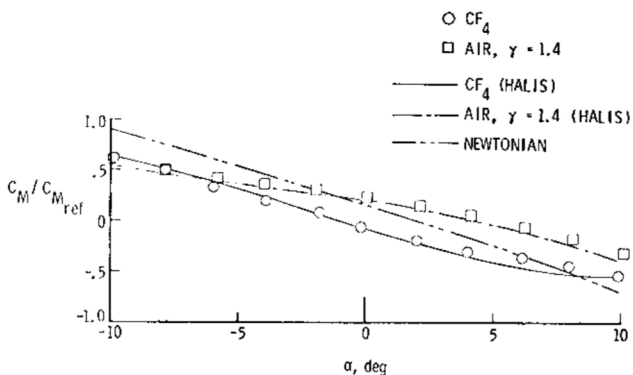


Fig. 3 Pitching moment for AFE configuration in Air at $M_\infty = 10$ and CF₄ at $M_\infty = 6$.

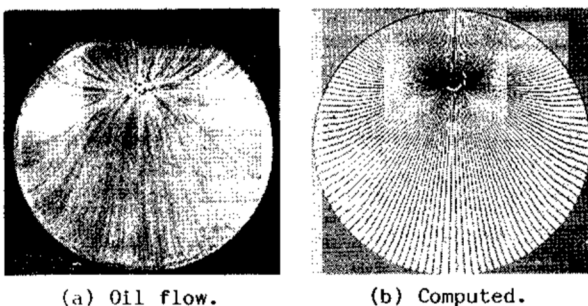


Fig. 4 Streamline pattern on AFE configuration at $\alpha = 0^\circ$.

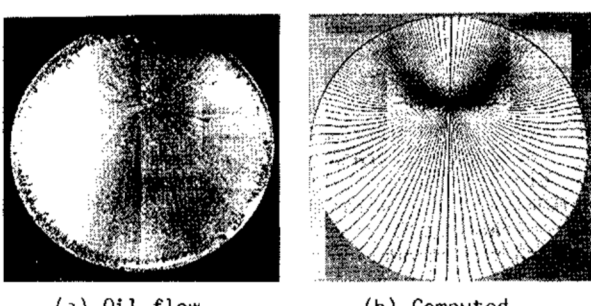


Fig. 5 Streamline pattern on AFE configuration at $\alpha = 5^\circ$.

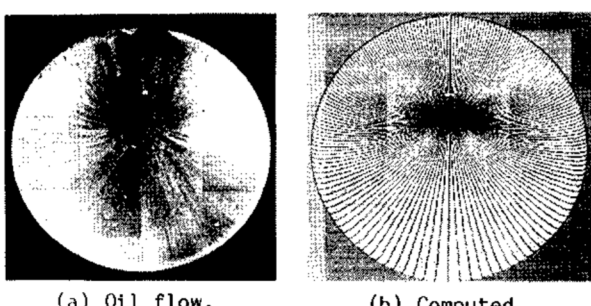


Fig. 6 Streamline pattern on AFE configuration at $\alpha = 10^\circ$.

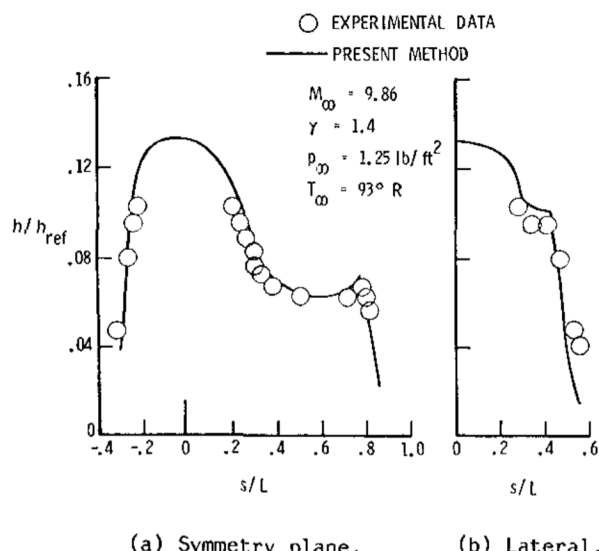


Fig. 7 Heating distribution on AFE configuration at $\alpha = 0^\circ$.

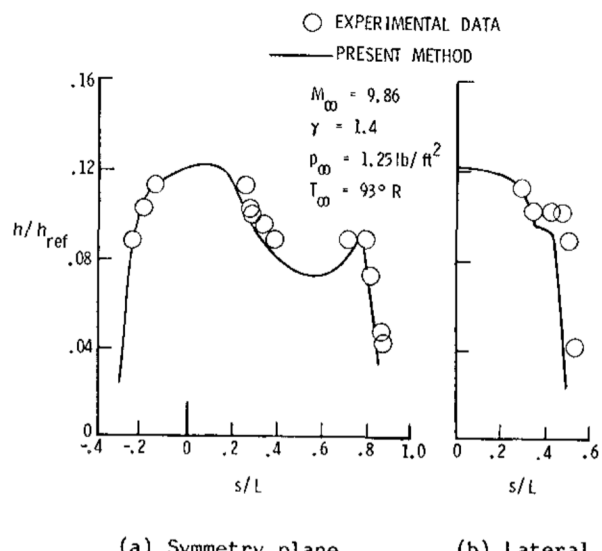


Fig. 9 Heating distribution on AFE configuration at $\alpha = 10^\circ$.

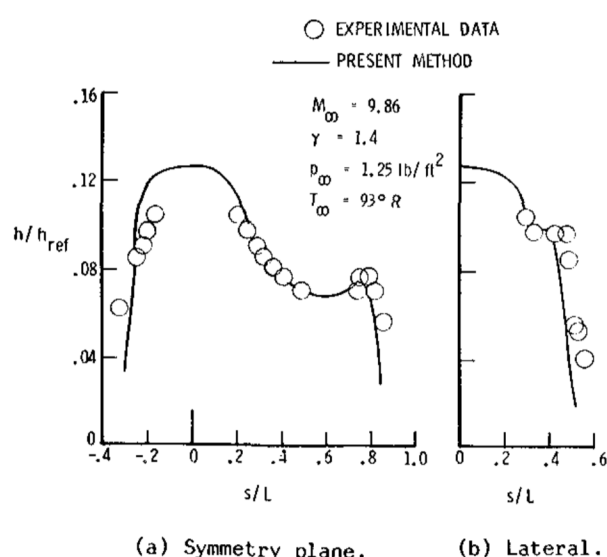


Fig. 8 Heating distribution on AFE configuration at $\alpha = 5^\circ$.

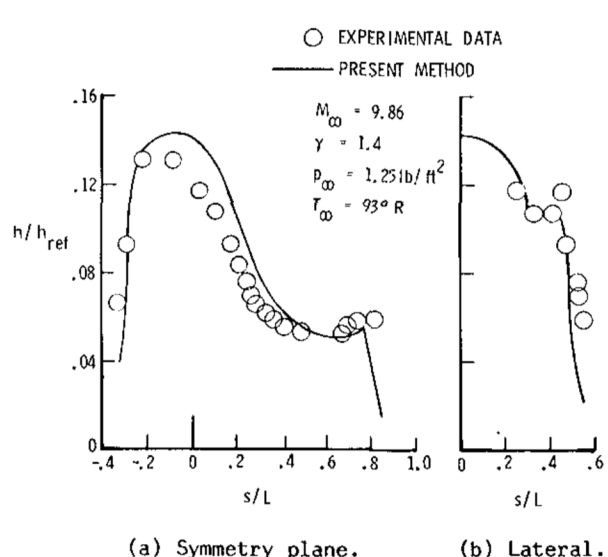
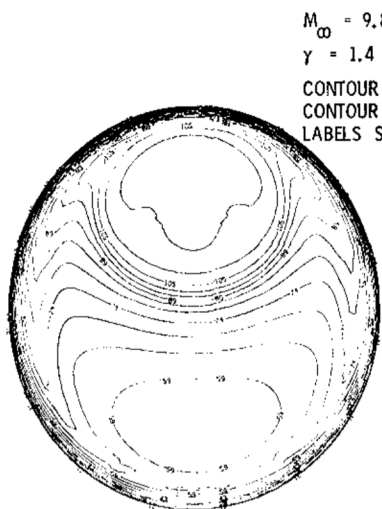
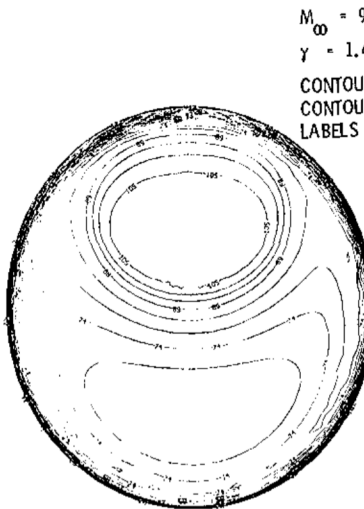


Fig. 10 Heating distribution on AFE configuration at $\alpha = -10^\circ$.



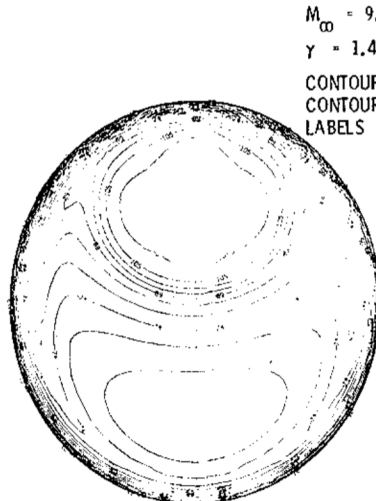
$M_\infty = 9.86$
 $\gamma = 1.4$
CONTOUR FROM 0.007 TO 0.11515
CONTOUR INTERVAL = 0.00515
LABELS SCALED BY 1000.0



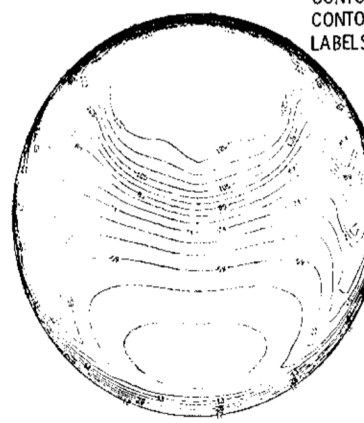
$M_\infty = 9.86$
 $\gamma = 1.4$
CONTOUR FROM 0.007 TO 0.11515
CONTOUR INTERVAL = 0.00515
LABELS SCALED BY 1000.0

Fig. 11 Heating contours on AFE configuration at $\alpha = 0^\circ$.

Fig. 13 Heating contours on AFE configuration at $\alpha = 10^\circ$.



$M_\infty = 9.86$
 $\gamma = 1.4$
CONTOUR FROM 0.007 TO 0.11515
CONTOUR INTERVAL = 0.00515
LABELS SCALED BY 1000.0



$M_\infty = 9.86$
 $\gamma = 1.4$
CONTOUR FROM 0.007 TO 0.12030
CONTOUR INTERVAL = 0.00515
LABELS SCALED BY 1000.0

Fig. 12 Heating contours on AFE configuration at $\alpha = 5^\circ$.

Fig. 14 Heating contours on AFE configuration at $\alpha = -10^\circ$.